# Correcting for Decorrelation Due to Atmospheric Phase Errors

M.A. Holdaway and F.N. Owen
National Radio Astronomy Observatory
Socorro, NM 87801

September 20, 1995

**Abstract**

We explore how image reconstruction degrades with uncorrected phase errors and how corrections can be made for the mean decorrelation even when we cannot correct for the actual phase errors. Correcting the visibility amplitude for the mean decorrelation as a function of baseline length improves the reconstructed image. Deconvolving the dirty image by a point spread function which includes the statistical effects of the phase errors as well as the effects of the incomplete Fourier plane sampling results in superior images. The latter technique permits very good image reconstruction even in the presence of phase errors as high as 70 degrees, and permits some sort of reconstruction in the presence of 105 degree rms phase errors. The MMA's phase error specifications need to be reevaluated in light of these new imaging techniques.

## 1 Introduction

Atmospheric phase errors cause trouble for millimeter interferometers: systematic phase errors result in gross positional errors; systematic and random phase errors limit the image quality; random phase errors limit the sensitivity through decorrelation of the visibilities; time dependent decorrelation results in flux scale errors; and since the phase errors (and hence decorrelation) grow worse with baseline, atmospheric phase errors limit the possible resolution of an array. The best line of defense against this tropospheric menace is to avoid the issue entirely by observing on a good site, on short baselines or at low frequencies where the phase errors will be lower. Since the science demands observations on long baselines and at high frequencies, we are pushed to use an active phase calibration technique which limits the residual phase errors to an acceptably low level. We have written about a specification of 30 degree rms residual phase error *per baseline* for any such exotic phase calibration technique (Holdaway, 1992). We think the strongest justification for this specification is the amplitude loss due to decorrelation given by $e^{-\sigma_\phi^2/2}$ (Thompson, Moran, and Swenson, 1986), where $\sigma_\phi$ is the rms phase error per visibility in radians. Hence, 30 degree rms phase errors will decrease the amplitude of the visibilities by 0.87. If the time scale of the phase fluctuations is larger than the integration time, the image flux will be down by 0.87, and the phase fluctuations will scatter flux through the image. However, this 13% loss in sensitivity is fairly modest, and we would probably be willing to live with a higher loss in sensitivity if we were performing exploratory observations at very high frequencies and we could somehow correct for the effects of the decorrelation. Hence, we should ask what level of phase errors will still permit reasonable imaging, and can anything be done to correct for the image errors caused by baseline dependent decorrelation?

## 2 Correcting for Decorrelation

Holdaway (1992) investigated image quality as a function of phase error magnitude for point sources and concluded that even with 30 degree rms phase errors, reasonable imaging with dynamic range of about 200:1 was still possible. In considering a more complex source, a more realistic atmospheric model with baseline dependent phase errors should be employed, as in the atmospheric simulations of Holdaway (1991). The particular atmospheric phase screen model used in the simulations described below results in phase errors which increase as the baseline raised to the 0.33 power, which is seen during good conditions on the potential MMA sites. During poorer conditions, the phase errors usually increase more steeply with baseline length, at least out to baselines of 300 m, but the basic conclusions derived from this work should be independent of the details of the phase structure function. Simulations were performed with a random circular array of 1 km maximum baseline. Samples on the $(u, v)$ tracks were calculated for 5 s integrations, the standard M31 HII region model image was Fourier transformed and degridded into the simulated $(u, v)$ points. We assumed no decorrelation occurred on time scales less than 5 s. The entire simulated data set was 18 minutes long, or ten atmospheric crossing times of the array's longest baseline. The amplitude of the phase screen was scaled as required, the phase screen was "blown" over the array with frozen turbulence at a velocity of 10 m/s, and the phase errors were then applied to the antennas below, thereby corrupting the phase of the visibilities. No other errors were added to the visibilities.

For the purpose of representing the typical level of phase fluctuations graphically, we parameterize each of the scaled atmospheres in the rms phase error calculated over the full 18 minute observation, averaged over all baselines. Hence, a model atmosphere with mean rms phase of 35 degrees will have some baselines with phase errors as high as 50 degrees.

We have imaged the corrupted visibilities in three different ways:

- we have imaged the source without any decorrelation correction, Fourier transforming the uniformly weighted gridded visibilities and deconvolving using the maximum entropy method (MEM) of Cornwell and Evans (1984).
- we have corrected the amplitudes of the target source visibilities based on the decorrelation observed in the calibrator source, followed by the Fourier transform and deconvolution.
- we have imaged the source by Fourier transforming the uncorrected visibilities and then deconvolving with a beam which includes both the effects of the sampling in the Foureir plane and the statistical effects of the phase errors.

We expound on the two correction techniques below.

### 2.1 Visibility Amplitude Correction

We have simulated calibrator observations which look through the same model atmosphere as the target source, but removed by more than 10 degrees on the sky. The details of the atmospheric phase time series detected by the calibrator are not applicable to the target source, and the target source visibilities have not been corrected for these phase errors. This is the typical state of current interferometer observations: the calibration is not fast enough to track the atmospheric phase errors. We average the calibrator visibilities to determine the extent of the decorrelation. The statistics of the phase errors on each baseline of the calibrator will be similar to the statistics of the phase errors on the target source, and the level of decorrelation will be comparable. Ignoring the phase of the averaged calibrator data, we can make a table of baseline based amplitude corrections given by

$$g_{i,j} = 1.0/AMP(1/N_t \sum_{k}^{N_t} V_{i,j}(t_k)). \tag{1}$$

We then average the target source visibilities to the same extent, increase the averaged target source visibilities' amplitudes by $g_{i,j}$, Fourier transform and deconvolve by the standard Fourier sampling based point spread function.

Averaging the visibilities in time will result in smaller phase errors, but will also limit the field of view, so this method will only work on smallish sources. The extent of the decorrelation and the resulting images will depend upon the averaging time used. In order to correct for the full $\exp^{-\sigma_\phi^2/2}$ decorrelation, we must average the visibilities over several baseline crossing times. The short baselines in our simulations are maximally decorrelated after averaging for a minute, while the 1 km baselines require averaging over the full 18 minute observation.

### 2.2 Statistical Deconvolution of Phase Errors

In radio astronomy, the Fourier transform of the sampled visibilities with no phase errors yields the dirty image

$$I_D(\mathbf{x}) = \sum V(\mathbf{u}_{i,j}) e^{i2\pi \mathbf{u}_{i,j}\cdot\mathbf{x}} \tag{2}$$

$$I_D(\mathbf{x}) = FT(V(\mathbf{u})S(\mathbf{u})), \tag{3}$$

where $V(\mathbf{u})$ is the visibility function and $S(\mathbf{u})$ is the sampling function. By the convolution theorem, multiplication by the sampling function $S(\mathbf{u})$ leads to a convolution of the true image by a point spread function which is given by the Fourier transform of $S(\mathbf{u})$. In the presence of antenna based phase errors $\phi_i$,

$$I_D(\mathbf{x}) = \sum V(\mathbf{u}_{i,j}) \cdot e^{i(\phi_i(t)-\phi_j(t))} e^{i2\pi \mathbf{u}_{i,j}\cdot\mathbf{x}}, \tag{4}$$

$$I_D(\mathbf{x}) = FT(V(\mathbf{u})S(\mathbf{u})T(\mathbf{u})), \tag{5}$$

where $T(\mathbf{u})$ represents the combined effects of the phases in the Fourier plane. Hence, the dirty image will be the true image convolved with a point spread function given by

$$PSF(\mathbf{x}) = FT(S(\mathbf{u})T(\mathbf{u})) = FT(S(\mathbf{u})) * FT(T(\mathbf{u})). \tag{6}$$

The problem with this formalism is that we do not know $T(\mathbf{u})$.

There is a nice analog to this approach in optical astronomical imaging, in which the resolution is limited by phase fluctuations in the atmosphere which are generally too fast to correct. A typical optical field of view contains several bright stars, and the profiles of these stars can be used to derive an effective point spread function representing the statistical effects of the atmosphere. The phase errors are occurring so quickly that we have thousands of independent instantiations of the phase errors, and even though the phase errors are not known in any detail, the form of $T(\mathbf{u})$ can be determined. Some degree of superresolution can then be achieved by deconvolving the effects of this point spread function from the entire image.

The situation at millimeter frequencies is different from the optical situation in two respects: we will have tens of crossing times of the turbulence over our aperture instead of thousands, and it will be rare to encounter bright point sources in the field of interest (Holdaway, Owen, and Rupen, 1994). Holdaway and Owen (1995) have recently analized the residual phase errors which result from imperfect atmospheric cancellation when switching between the target source and a nearby calibrator. Phase fluctuations which occur faster than the switching time scale cannot be corrected, and will result in significant decorrelation if the residual phase errors are about 30 degrees or larger. However, it is possible to use the statistics of the phase errors as measured on a calibrator to simulate an effective point spread function which would include the effects of both the incomplete Fourier sampling and the phase jitter. We can determine the phase structure function from the calibrator phase time series, which allows us to construct a model phase screen which will have the same statistical properties as the actual atmosphere, but which will not have the correct detailed phases. Hence, deconvolving with the point spread function which includes phase errors from this model atmosphere can correct for the decorrelation, as can the amplitude correction scheme. As in the amplitude correction scheme, details of the phase time series derived from the model atmosphere will be wrong, so errors will be made. However, on average, the model phases will affect the point spread function in a manner which is representative of how the actual target source phase errors scatter flux in the target source. We found that superior results were achieved when we calculated the effective point spread function, including phase errors, from several (ten) different model atmospheres, averaged the different model point spread functions, and then deconvolved the dirty image with this effective point spread function.

This method, or the *statistical deconvolution of phase errors*, is quite similar to correcting the decorrelated amplitudes. After averaging several effective PSF's, the phases will be small, so the effective PSF will be dominated by the Fourier sampling and the amplitude decorrelation. Consider the case of perfect Fourier sampling, so the effective PSF is due entirely to the amplitude decorrelation. Deconvolving by this function is equivalent to dividing the Fourier transform of the image by the Fourier transform of the effective PSF, or boosting up the amplitudes of the outer visibilities as performed when correcting the decorrelated amplitudes.

In both the amplitude correction and the statistical deconvolution of phase errors schemes, the results are dependent upon the post observation averaging time in a complicated manner which has not yet been fully explored.

### 2.3 Comparing the Methods

We can compare the success of these various imaging pathways on a wide range of simulated data through standard measures of imaging success such as the dynamic range and fidelity index, or more subjectively through looking at the final reconstructions side by side. The fidelity image, first introduced by Cornwell, Holdaway, and Uson (1993) to measure the success of image simulation, is an image of the quantity one over the fractional pixel error. The fidelity index, renamed here as the *median fidelity*, is the median pixel value of the fidelity image after clipping the low fidelity points which occur in very faint pixels and pixels whose fidelity is very high by chance. Since most pixels in our model images are fairly low brightness, the median fidelity emphasizes the great sea of low brightness pixels. A reconstruction with a median fidelity of 20 is considered highly successful. For the current investigation, we further define the first moment of the fidelity, which is the mean fidelity weighted by the pixel value raised to the first power. The first moment fidelity is less sensitive to errors in the low brightness pixels and better gauges the success of the reconstruction of the bright, compact features in the image. Both fidelities measure the quality of image reconstruction *on source*, while the dynamic range measures the level of error *off source* relative to the brightest reconstructed feature.

Figure 1 shows the images of a series of simulations with 17°, 35°, 70°, and 105° rms phase errors, reconstructed with no correction, with the statistical phase deconvolution, and with the the visibility amplitudes corrected. As can be seen in the first column, as the phase errors increase, the detailed structure of the source gets smeared and the flux scale goes down. In the two correction techniques, the right flux scale is maintained even in the presence of the largest phase errors. However, inconsistencies in the amplitude corrected data scatter flux all over the image, limiting the dynamic range as well as the fidelity of the image. The statistical phase deconvolution method appears to be superior and results in a very good reconstruction even with 70 degree rms phase errors. Note that the point spread function used in the statistical phase deconvolution method embodies both the loss in resolution and the loss in sensitivity since the phase errors are spreading the beam about and even cancelling part of the beam flux. The resolution and sensitivity loss are represented as a function of phase error in Figure 2. Finally, the dynamic range and fidelities are plotted for each reconstruction scheme as a function of rms phase error in Figure 3.

## 3 Implications for the MMA

Under the assumption of baseline independent Gaussian residual phase errors, such as might exist if Welch's total power monitor scheme or Woody's water vapor spectrometer scheme were employed, a simpler decorrelation correction might suffice. If the residual phase errors were antenna dependent or time dependent, then one of the decorrelation correction methods described here might improve the imaging.

In the case of fast switching, the residual phase errors are equal to the square root of the phase structure function $\sqrt{D_\phi(\rho)}$ for short baselines $\rho$ and saturate at a value of $\sqrt{D_\phi(vt/2+d)}$ for baselines longer than the effective switching length $vt/2+d$ (Holdaway and Owen, 1995). Since the decorrelation is baseline dependent under fast switching, the decorrelation correction methods described above would be helpful.

Currently, it is believed that reasonable imaging with the 40 element mma should be possible with 30 degree rms phase errors, assuming the phase errors do not maintain some systematic value over long times. The 30 degree rms phase error per baselines specification comes from point source simulations (dynamic range = 200:1; Holdaway, 1992) and from sensitivity arguments (down to 0.87). These simulations show that the MMA will be able to make high fidelity, moderate dynamic range images of complex sources with rms phase errors of 70 degrees per baseline (the worst baselines in this simulation actually had rms phase errors of 100 degrees). The 70 degree phase errors will result in a stiff penalty in sensitivity since the decorrelation is down to 0.47 on the typical baseline. A modest resolution loss of 17% also occurs.

We propose that we have two levels of phase error specifications:

- The primary phase error specification of 30 degrees rms per baseline will permit excellent imaging with almost no loss in sensitivity from decorrelation. This should be the primary goal of our phase correction schemes.

- The secondary phase error specification of 70 degrees rms per baseline will still permit very good imaging with a loss of 50% in sensitivity (a factor of four in time). This secondary phase error specification reminds us that atmospheric conditions which do not allow us to meet the primary phase error specification are not lost. This will be particularly important for an instrument which is built on a suboptimal site and for observations at very high frequencies.

In Table 4 we explore what the 30 degree and 70 degree phase error specifications mean for observing on a 300 m baseline at Chajnantor in Chile *without any phase calibration*. We list the phase stability quartiles measured on the NRAO 300 m, 11.2 GHz site test interferometer for the month of June 1995, and then determine what frequency can be observed with 30 degree and 70 degree phase errors. Fast switching can achieve an effective calibration baseline $vt/2+d$ of about 50 m (Holdaway and Owen, 1995), and typical phase structure function power law exponents are 0.7, so the post-calibration phase errors would be $(50/300)^{0.7} = 0.29$ lower than the rms phase errors measured on the 300 m baseline. These lower phase errors would pertain to all baselines longer than 50 m, and would boost the peak observing frequencies given in Table 4 by a factor of 3.5.

## 4 Acknowledgements

Special thanks to Claire Chandler who motivated this project, and may yet let her name be on the auther list. Also, praise and thanks to Michael Rupen and Tim Cornwell for nice but not yet implemented ideas. And thanks to Scott Foster for technical support.


**References**


Cornwell, T.J., and Evans, 1984. A&A,

Cornwell, T.J., Holdaway, M.A., and Uson, J., 1993, A&A.

Holdaway, M.A, 1991, MMA Memo 68, "A Millimeter Wavelength Phase Stability Analysis of the South Baldy and Springerville Sites".

Holdaway, M.A., 1992, MMA Memo 84, "Possible Phase Calibration Schemes for the MMA".

Holdaway, M.A., Owen, F.N., and Rupen, M.P., 1994, MMA Memo 123, "Source Counts at 90 GHz".

Holdaway, M.A., and Owen, F.N., 1995, MMA Memo 126, "A Test of Fast Switching Phase Calibration with the VLA at 22 GHz".

Holdaway, M.A., Radford, Simon J.E. , Owen, F.N., and Foster, Scott M., 1995, MMA Memo 129, "Data Processing for Site Test Interferometers".

Thompson, A. Richard, Moran, James M., and Swenson, George W., *Interferometry and Synthesis in Radio Astronomy*, John Wiley & Sons, New York, 1986.

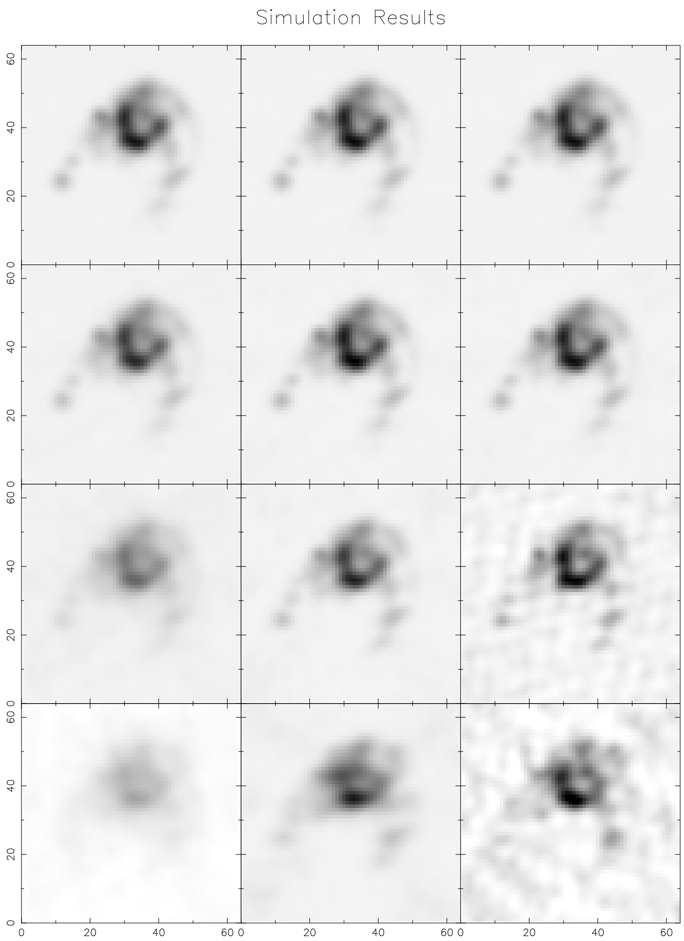


Figure 1: Three different reconstruction techniques (columns) applied to four different magnitudes of phase errors (rows). *Column 1*: imaging without any decorrelation correction. *Column 2*: imaging with the statistical phase deconvolution. *Column 3*: imaging with correction of the amplitudes only. *Row 1*: 17 degree rms phase errors. *Row 2*: 35 degree rms phase errors. *Row 3*: 70 degree rms phase errors. *Row 4*: 105 degree rms phase errors. The statistical phase deconvolution technique is superior for large phase errors.

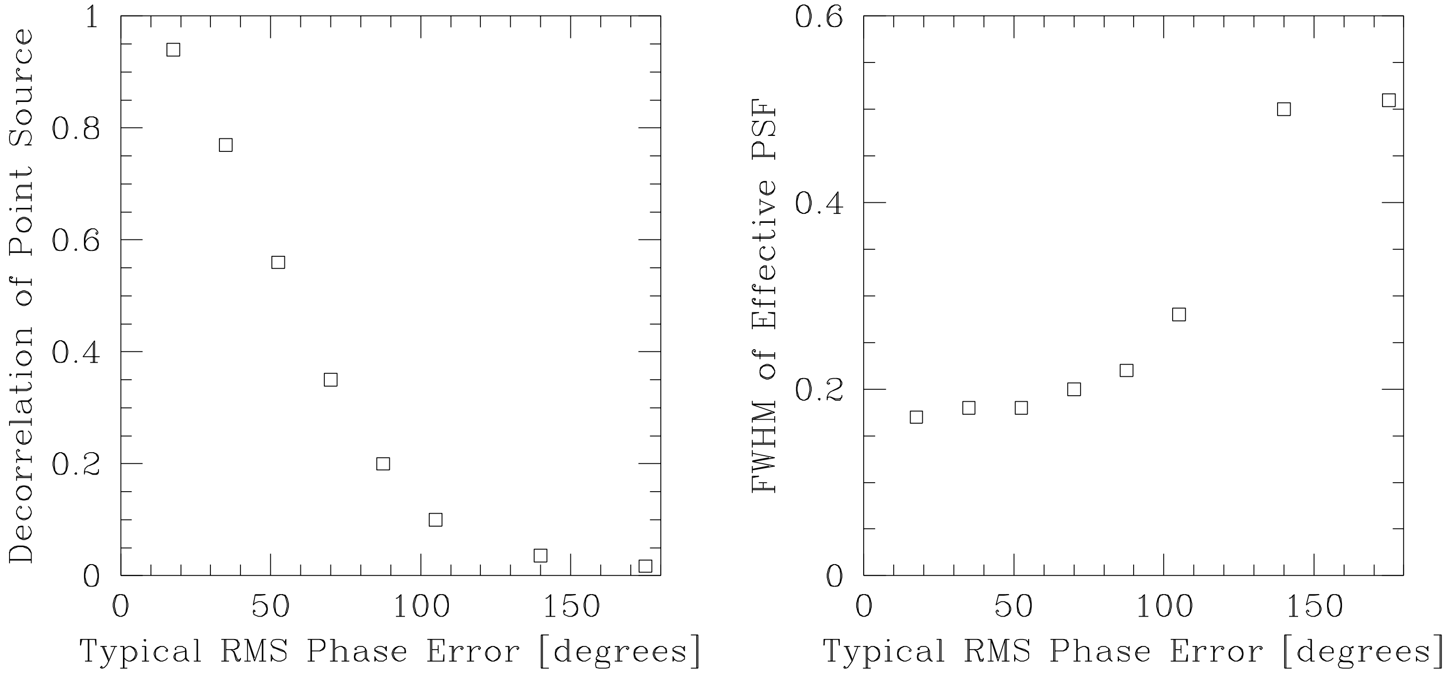


Figure 2: The phase errors will degrade the resolution as well as the sensitivity. These figures illustrate how the resolution and sensitivity at the highest resolution degrade with increasing phase errors in our simulations. The sensitivity curve is consistent with $\exp^{-\sigma_\phi^2/2}$ when we consider that the phase errors at the highest resolution are higher than the mean phase errors we plot. Also, the beam fitting is ill-conditioned in the high phase error case, which explains why the resolution seems to flatten out at the right side of the graph.

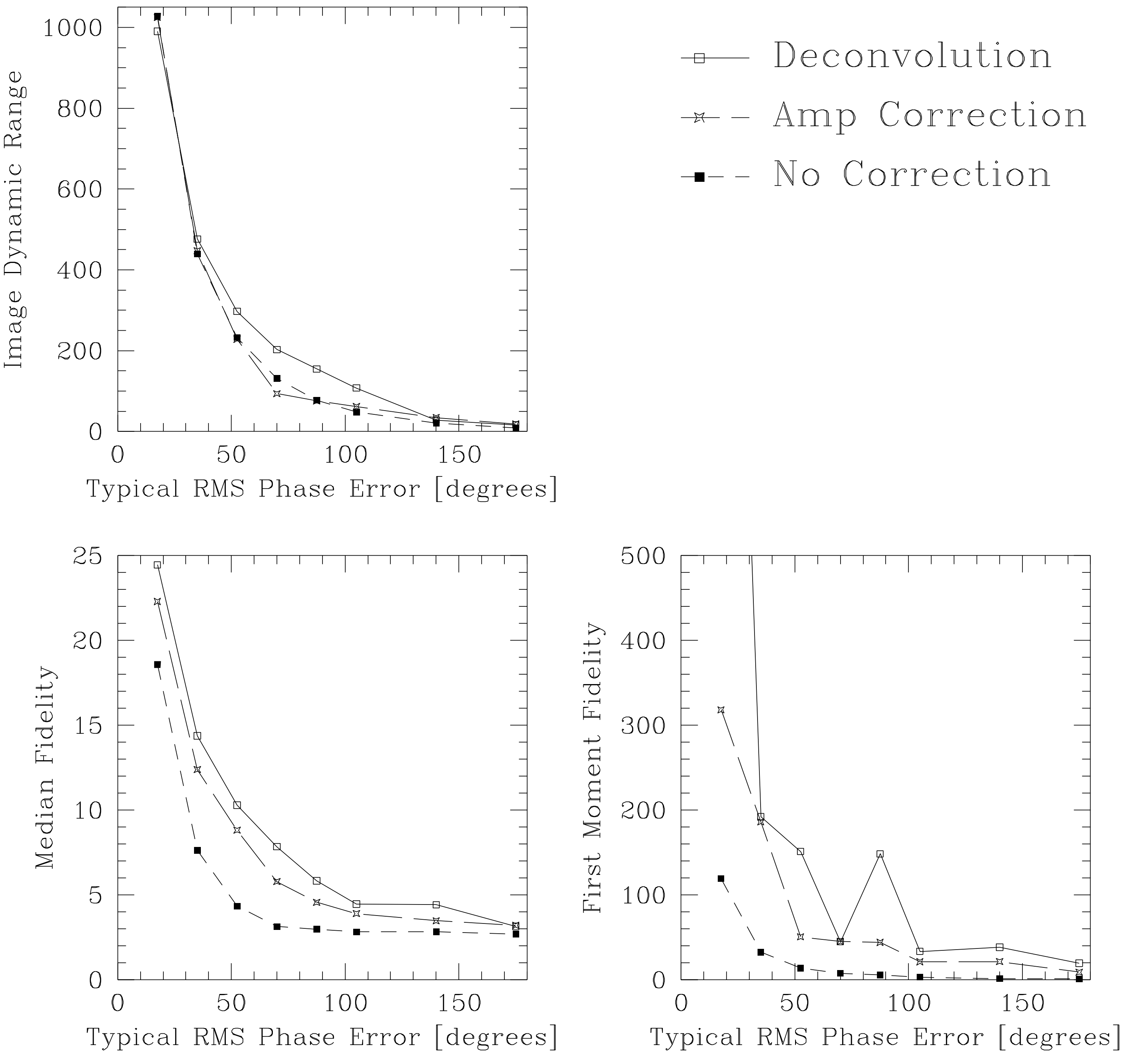


Figure 3: Three measures of image quality for the three imaging methods compared in this memo: (a) Dynamic Range, defined as the image peak divided by the off-source rms, (b) Median Fidelity, defined in the text, and (c) First Moment Fidelity, defined in the text.

| Fraction of time | $\sigma_\phi$ at 11.2 GHz | $\nu$ at which $\sigma_\phi = 30°$ | $\nu$ at which $\sigma_\phi = 70°$ |
|---|---|---|---|
| 0.75 | 2.95° | 113 GHz | 266 GHz |
| 0.50 | 1.61° | 209 GHz | 487 GHz |
| 0.25 | 0.93° | 361 GHz | 843 GHz |
| 0.10 | 0.66° | 509 GHz | 1190 GHz |

Table 1: How high a frequency could you operate the MMA in Chile if 30 degree rms phase errors were required, and if 70 degree rms phase errors were required? We present here the very conservative estimates based on the NRAO 300 m, 11.2 GHz site test interferometer data taken for the month of June 1995. The phase at 11.2 GHz was better than 2.95 degrees 75% of the time, indicating that 113 GHz observations would have phase errors of less than 30 degrees more than 75% of the time, and 266 GHz observations would have phase errors of less than 70 degrees more than 75% of the time. This table does not consider any form of calibration aside from the decorrelation corrections described in this memo. Active phase calibration could increase the maximum frequencies quoted in this table by a factor of 3.5.